Proceedings of ICBioMed 2025 Symposium: AI for Healthcare: Advanced Medical Data Analytics and Smart Rehabilitation
DOI: 10.54254/2753-8818/2025.AU27080

CTNNA3 and MBP Mediate Treatment Resistance Through Tumor Microenvironment Remodeling in Recurrent Glioblastoma

Wenna Mao

Milton Academy, Milton, USA
wenna_mao26@milton.edu

Abstract. Glioblastoma multiforme represents the most common primary malignant brain tumor in adults, with a 90% 2-year recurrence rate despite standard therapy of surgical resection followed by chemo- and radiotherapy. Yet, the cellular mechanisms underlying therapeutic resistance remain poorly understood. By integrating analysis of single-cell RNA sequencing results of 41 primary and 43 recurrent tumor specimens with experimental validation, we identify neuro-oligodendrocyte precursors as the predominant cellular population driving tumor recurrence through establishment of protective microenvironmental niches. We discover that CTNNA3 and MBP exhibit paradoxical roles in promoting survival in primary tumors while conferring chemoresistance in recurrent GBM, revealing that these factors determine treatment efficacy rather than directly driving relapse. Functional assays confirmed their role as mediators of extracellular matrix remodeling, establishing a mechanistic link between tumor microenvironmental remodeling and therapeutic resistance. By revealing how recurrent tumors engineer self-protective niches, our study provides a new framework for developing combination therapies that disrupt these resistance mechanisms and provides foundation for overcoming treatment failure in this universally fatal disease.

Keywords: Glioblastoma, tumor microenvironment, CTNNA3, MBP, GBM recurrence

1. Introduction

Glioblastoma multiforme (GBM) is the most common primary brain tumor in adults, with a five-year survival rate of approximately 5% [1]. The incidence of GBM has been increasing globally, with rises reported across South America and Europe as of 2017 [2]. Traditional treatment involves surgical resection followed by concurrent chemotherapy with temozolomide and radiotherapy [3]. However, this method has yielded limited success. 90% of patients experience tumor recurrences within two years of initial surgery, presenting an urgent need for more effective treatment of relapsed GBM [4].

The advent of Single-Cell RNA Sequencing (scRNA-seq) in 2009 advanced researchers' ability to dissect intricate expression profiles and understand tumor biology at the higher single-cell resolution [5, 6]. This technology has revolutionized our ability to examine tumor heterogeneity and

© 2025 The Authors. This is an open access article distributed under the terms of the Creative Commons Attribution License 4.0 (https://creativecommons.org/licenses/by/4.0/).

DOI: 10.54254/2753-8818/2025.AU27080

identify cellular changes that occur during disease progression [7]. Wang et al. performed single-nucleus RNA sequencing on 86 tissue specimens from 49 GBM patients. Their dataset included paired specimens from primary untreated tumors and matched first recurrences from 36 patients, providing a valuable opportunity to understand recurrent GBM [8].

In our study, we analyzed the Wang et al. dataset to further understand GBM relapse. Our computational analysis identified CTNNA3 and MBP among the top five upregulated genes in recurrent versus primary GBM, with predominant expression observed in neuro-oligo precursor cells (OPCs). CTNNA3 encodes αT-catenin, a critical component of the cadherin-catenin complex that regulates cell-cell adhesion and facilitates signaling between the extracellular matrix and intracellular pathways [9, 10]. MBP (myelin basic protein) is an essential structural component of the myelin sheath that facilitates cytosolic membrane adhesion and can interact with extracellular matrix components and cell surface receptors to transduce signals between the extracellular environment and intracellular pathways [11]. To validate these computational findings, we performed functional assays using GBM cell lines treated with TMZ and supplemented with CTNNA3 and MBP proteins. Wound healing assays, CCK-8 viability assays, and immunofluorescence analyses confirmed that these proteins enhance cell migration, survival, and extracellular matrix (ECM) protein expression.

Integrating computational analyses with wet lab validation may help pinpoint potential genes and pathways for the development of combination therapies. Such insights could improve survival outcomes for GBM patients.

2. Methodology

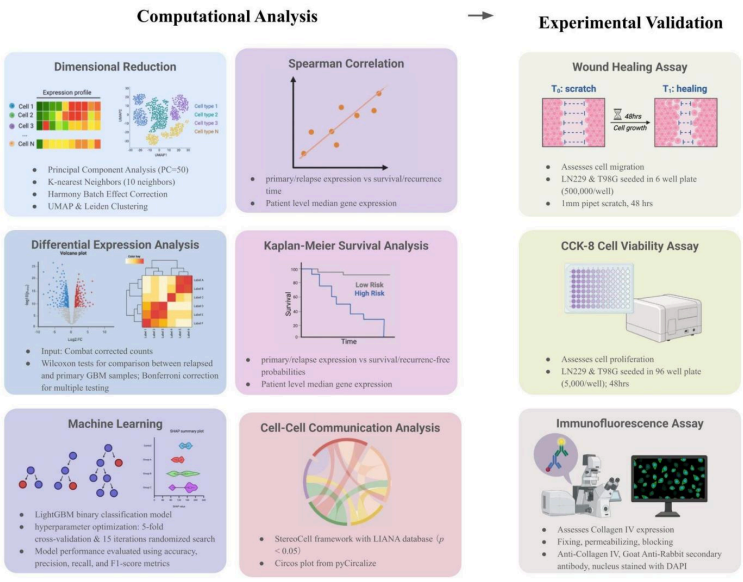


Figure 1. Workflow of the study. Figure was created with BioRender.com

2.1. Data acquisition

Single-nucleus RNA sequencing data from Wang et al. was obtained from the Gene Expression Omnibus (GEO) database under accession number GSE174554. The dataset includes a cohort with ages ranging from 35 to 76 years and a male-to-female ratio of 1.2 [8].

DOI: 10.54254/2753-8818/2025.AU27080

2.2. Preprocessing

Raw count data were compiled into an AnnData object for downstream analysis. Quality control filtering was applied to retain genes expressed in at least 3 cells and cells expressing a minimum of 200 genes. Cells with mitochondrial gene expression exceeding 15% were excluded to remove low-quality nuclei. Additional filtering removed cells expressing in the upper and lower 2 quantiles, eliminating outliers and low-quality cells. Doublet detection was performed using Scrublet with default parameters.

Following quality control, count data were normalized to 10,000 total counts per cell and log-transformed (log(count + 1)) to stabilize variance. The top 3,000 highly variable genes were identified based on normalized dispersion to focus on genes driving biological variation.

2.3. Batch effect correction & dimensional reduction

Batch effects arising from different patients and processing batches were corrected using two complementary approaches: Combat for count-level correction and Harmony for latent space integration. Total counts and mitochondria gene percentage were regressed out, and gene expression values were scaled to unit variance for dimensional reduction.

Principal Component Analysis (PCA) was performed using the top 3,000 highly variable genes, and Harmony corrected the top 18 principal components for downstream analysis. k-nearest neighbor was performed with k = 10 neighbors. Uniform Manifold Approximation and Projection (UMAP) was applied for dimensional reduction.

2.4. Clustering and cell type annotation

Unsupervised clustering was performed using the Leiden algorithm at 0.7 resolution to identify distinct cell populations. Cell type identity was determined through manual annotation based on expression of established marker genes and comparison with known GBM cell type signatures.

2.5. Differential expression analysis

Differential gene expression between primary and recurrent tumors was assessed using the Wilcoxon rank-sum test implemented in Scanpy. To account for multiple testing, Bonferroni correction was applied with a significance threshold of adjusted p-value < 0.05. Genes were ranked by the product of log fold change and negative log p-value to prioritize both statistical significance and expression change (minimum p-value was set to 1×10^{-300} to avoid computational overflow).

2.6. Feature selection and modeling

A Light Gradient Boosting Machine (LightGBM) Classification model was used to predict genes that differentiate cells from primary to relapse. Hyperparameter optimization was performed using 5-fold cross-validation and randomized search over 15 iterations, resulting in the following parameter configurations: colsample_bytree = 0.687, learning_rate = 0.200, max_depth = 5, n_estimators = 171, num_leaves = 26, and subsample = 0.723. For each cross-validation fold, model performance was evaluated using matrix accuracy, precision, recall, and F-1 scores. The contributions of each feature to model prediction were assessed using Shapley Additive exPlanations (SHAP) Tree Explainer framework. Features were ranked based on their mean absolute SHAP values, and the top 20 significant genes were visualized using SHAP summary plot.

DOI: 10.54254/2753-8818/2025.AU27080

2.7. Survival and correlation analysis

For survival analysis, patient-level gene expression was calculated as the median expression across all cells for each patient. Spearman's rank correlation was computed between gene expression and patient survival/recurrence time, performed separately for primary and recurrent tumor groups. Statistical confidence was assessed using t-statistics derived from correlation coefficients.

Kaplan-Meier survival analysis was performed to compare survival probabilities between patient groups stratified by gene expression levels. Patients were stratified into high and low expression groups based on median gene expression values. Survival curves were compared using the log-rank test, with p-values < 0.05 considered statistically significant. Statistical power was calculated for both correlation and survival analyses to assess the adequacy of the sample size.

2.8. Cell-cell communication analysis

Cell-cell communication analysis was used to explore potential ligand-receptor interactions underlying functional differences between primary and relapsed groups. The analysis was performed using the StereoCell framework with a p-value threshold of 0.05 for statistical significance. Cellular interactions were identified by leveraging the LIANA database of human ligand-receptor pairs. Figures were generated using Circos from Pycircalize. Each plot represents interactions within 2 specific cell types.

2.9. Cell culture, reagents, and antibodies

Human GBM cell lines LN229 and T98G were obtained from the American Type Culture Collection (ATCC) and maintained in Dulbecco's Modified Eagle Medium (DMEM; Anweisci, Shanghai, China) supplemented with 10% fetal bovine serum (FBS; BI, Beijing, China) at 37°C. Anti-collagen IV rabbit antibody and goat anti-rabbit IgG H&L (Alexa Fluor® 488) secondary antibody were purchased from Abcam (Shanghai, China). Cell Counting Kit-8 (CCK-8) solution was obtained from Vazyme (Shanghai, China). 4% paraformaldehyde and DAPI (4',6-diamidino-2-phenylindole) were purchased from Biosharp (Shanghai, China). Recombinant CTNNA3 and MBP proteins were obtained from LB (Beijing, China) and dissolved in PBS to a stock concentration of 1 mg/mL and stored at 4°C. Temozolomide (TMZ) was dissolved in dimethyl sulfoxide (DMSO) to a stock concentration of 1 mM and stored at 4°C.

2.10. Wound healing assay

Cell migration ability was assessed using wound healing assay. LN229 and T98G cells were seeded in 6-well plates at a density of 500,000 cells per well and cultured overnight to reach confluence. Uniform scratches were created perpendicular to the monolayer using a sterile 1 mL pipette tip. Cellular debris was removed by washing three times with PBS, and wells were treated with 300 μM TMZ in DMEM (or DMEM alone as negative control) along with recombinant proteins (CTNNA3, MBP, or both) at concentrations of 0.1, 0.3, and 1.0 μg/mL. Cells were incubated for 48 hours at 37°C. All experiments were performed in triplicate ($n = 3$). Wound closure was monitored and photographed at 0 and 48 hours using a Qibu inverted microscope. Healing rate was calculated using [(initial scratch width - final scratch width) / initial scratch width] × 100%.

DOI: 10.54254/2753-8818/2025.AU27080

2.11. CCK-8 assay

Cell viability was measured using the CCK-8 assay. LN229 and T98G cells were seeded in 96-well plates at 5,000 cells per well and allowed to adhere overnight. Cells were then treated with 300 μM TMZ in DMEM (or DMEM alone as negative control) and recombinant proteins at concentrations of 0.1, 0.3, and 1.0 μg/mL for 48 hours at 37°C. Following treatment, 10 μL of CCK-8 solution was added to each well, and plates were incubated for 1 hour at 37°C. All experiments were performed in triplicate (n = 3). Optical density was measured at 450 nm using a Qibu microplate reader. Cell viability was expressed as a percentage relative to untreated controls.

2.12. Immunofluorescence analysis

For immunofluorescence staining of collagen IV, GBM cells were seeded in 12-well plates at 100,000 cells per well and cultured overnight. Cells were treated with 300 μM TMZ in DMEM (or DMEM alone as negative control) and 1 μg/mL recombinant proteins (except for the positive control group). Following treatment, cells were fixed with 4% paraformaldehyde for 15 minutes at room temperature, permeabilized with 0.5% Triton X-100 for 20 minutes, and blocked with 2% bovine serum albumin (BSA) for 30 minutes at room temperature. Cells were incubated with primary anti-collagen IV antibody (1:1000 dilution) overnight at 4°C. After washing with PBS, cells were incubated with Alexa Fluor® 488-conjugated goat anti-rabbit secondary antibody (1:1000 dilution) for 1 hour at room temperature in the dark. Nuclei were stained with DAPI (1 μg/mL) for 5 minutes. All experiments were performed in triplicate (n = 3). Fluorescence images were captured using an ECHO fluorescence microscope.

3. Results

3.1. Computational results

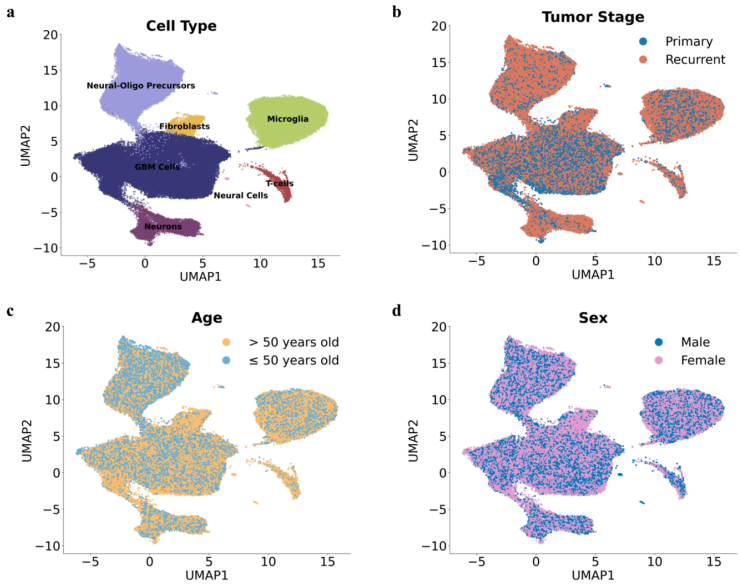


Figure 2. UMAP embedding colored by (a) cell type, (b) tumor stage, (c) age, and (d) sex

DOI: 10.54254/2753-8818/2025.AU27080

UMAP dimensional reduction revealed distinct cellular populations within GBM tumors, including GBM cells, neuro-oligo precursor cells (OPCs), neurons, fibroblasts, microglia, T-cells, and other neural cell types (Figure 2a). While most cell populations showed relatively balanced representation between primary and recurrent tumors, a notable population of recurrent tumor cells was observed within the OPC and fibroblast clusters (Figure 2b). The fibroblast cluster is also made of a notable population of cells from female patients and patients older than 50 (Figure 2c, 2d).

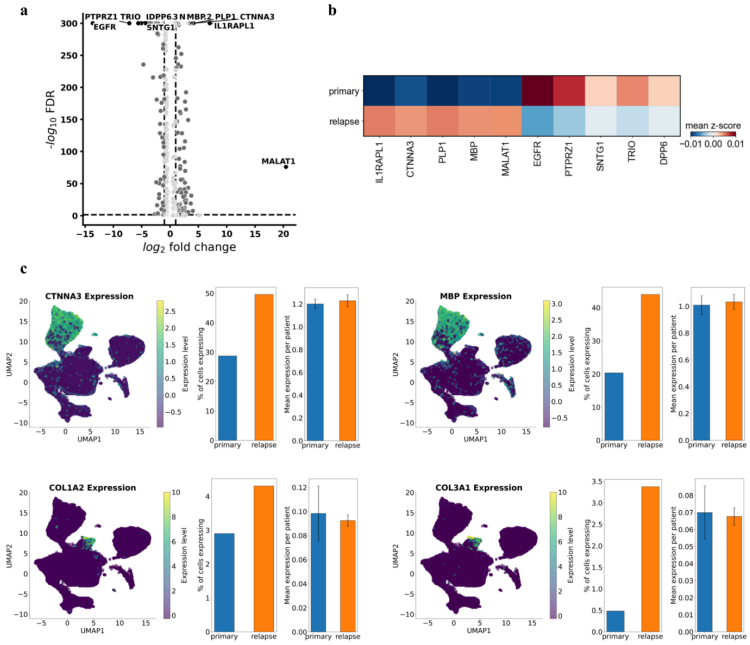


Figure 3. (a) Volcano plot showing differentially expressed genes between primary and recurrent tumors, with log fold change as x-axis and adjusted p-value as y-axis. The top five upregulated genes and downregulated genes are labeled. (b) Heatmap displaying normalized expression of the ten most differentially expressed genes across primary and recurrent tumor samples. (c) UMAP visualization of CTNNA3, MBP, COL1A2, and COL3A1 expression. Bar plots show percentage of expressing cells (left, raw counts) and mean patient-level expression (right, ComBat-corrected counts) for primary (n = 30) vs. recurrent (n = 42) tumors. Data shown as mean ± SD. Wilcoxon rank-sum test with Bonferroni correction was used for statistical testing

Differential gene expression analysis between primary and recurrent GBM identified IL12RAPL1, CTNNA3, MBP, PLP1, and MALAT1 as the top 5 upregulated genes based on both change in expression and statistical significance (log fold change × p-value) (Figure 3a). Of particular interest, CTNNA3 and MBP are both associated with cell migration and adhesion processes, making them compelling candidates for functional validation (Figure 3a). Conversely, EGFR, PTPRZ1, SNTG1, TRIO, and DPP6 were among the five most downregulated genes in recurrent versus primary GBM (Figure 3a). The heatmap validates the volcano plot and demonstrates clear expression patterns in previously identified genes that distinguish recurrent from primary tumors (Figure 3b). UMAP visualization revealed that CTNNA3 and MBP are expressed predominantly in neuro-oligo precursor cells (OPCs) (Figure 3c). They are expressed in a higher percentage of cells in recurrent tumors, and their mean expression levels per patient are elevated compared to primary tumors (Figure 3c). COL1A2 and COL3A1 are also expressed in a higher

DOI: 10.54254/2753-8818/2025.AU27080

percentage of cells in recurrent tumors, however, their mean expression per patient in relapse lowered compared to primary (Figure 3c).

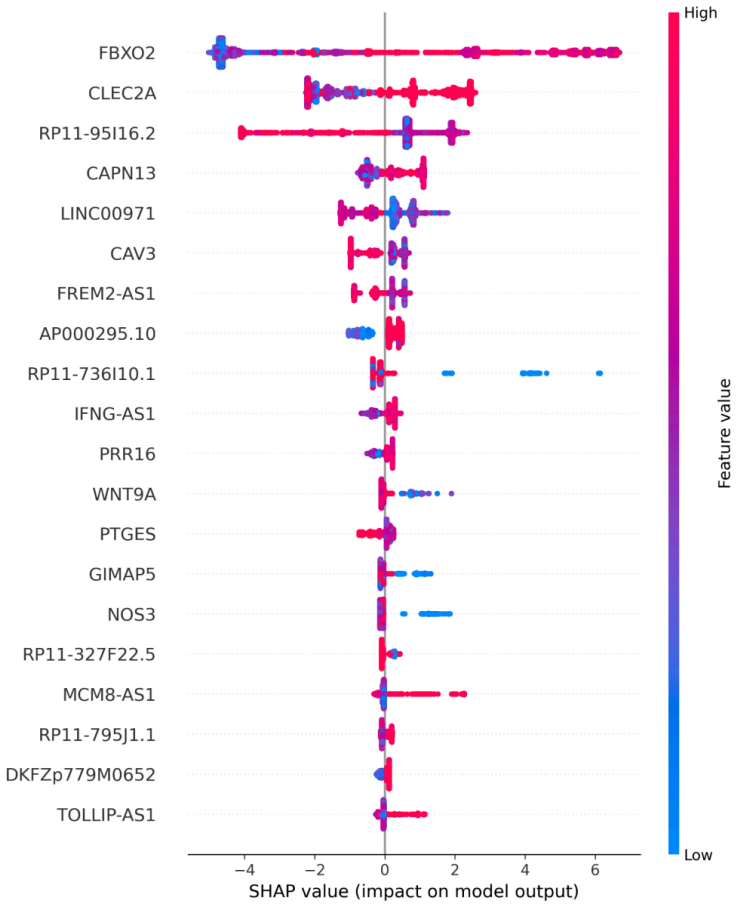


Figure 4. SHAP summary plot demonstrating the impact of the top 20 genes on LightGBM classification model output for predicting primary versus relapse tumors. Hyperparameter optimization was performed using 5-fold cross-validation with randomized search over 15 iterations. The x-axis represents SHAP values (contribution to model output), with positive values indicating contribution toward relapse and negative values toward primary GBM classification. The y-axis lists genes ranked by mean absolute SHAP values. Color represents feature value

Machine learning analysis using LightGBM identified the genes most predictive of tumor recurrence status. FBXO2 demonstrated the highest mean absolute SHAP value, with elevated expression strongly associated with recurrent tumor classification (Figure 4). Additional genes contributing significantly to recurrence prediction included CLEC2A and CAPN13, while RP11-951I16.2 and LINC00971 were more predictive of primary tumor status. Notably, WNT9A, a key ligand in the Wnt signaling pathway involved in stem cell proliferation and maintenance, showed moderate predictive value with variable contributions to both primary and recurrent classifications (Figure 4). FBXO2, CLEC2A, and CAPN13 are collectively associated with cellular adhesion, motility, and extracellular matrix remodeling processes [12-14].

DOI: 10.54254/2753-8818/2025.AU27080

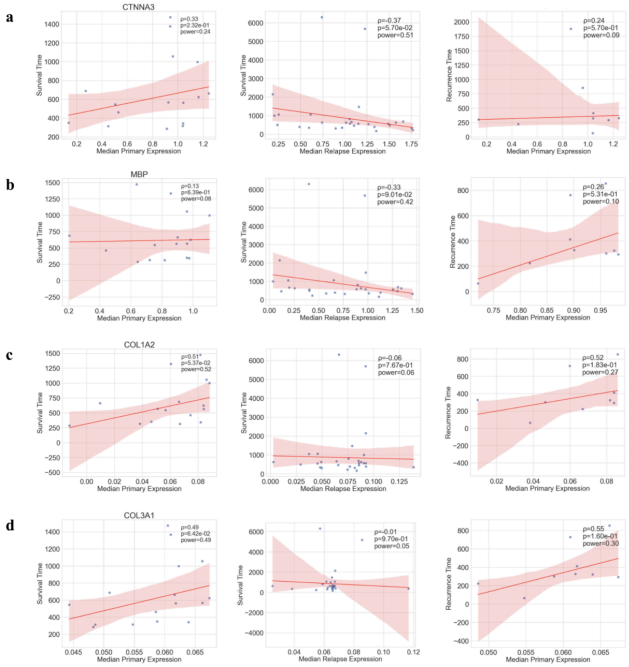


Figure 5. Spearman correlation plots show relationships between median gene expression levels (per patient) and clinical outcomes for (a) CTNNA3, (b) MBP, (c) COL1A2, and (d) COL3A1. For each gene, three analyses were conducted: correlation with survival time in primary tumors (left column, n = 15), correlation with survival time in recurrent tumors (middle column, n = 27), and correlation with recurrence time in primary tumors (right column, n = 8). Each point represents an individual patient

Correlation analysis revealed distinct patterns between gene expression and clinical outcomes depending on tumor stage. In primary tumors, higher expression levels of CTNNA3, MBP, COL1A2, and COL3A1 demonstrated positive correlations with both patient survival time and time to recurrence, suggesting potential protective effects in the primary disease setting (Figure 5). However, these correlations did not reach statistical significance, likely due to insufficient statistical power. Low statistical power was observed for several correlations: primary CTNNA3 expression versus recurrence time (power = 0.09, n = 8), primary MBP expression versus survival time (power = 0.08, n = 15), and both relapse COL1A2 and COL3A1 expression versus survival time (power = 0.06 and 0.05, respectively, n = 27) (Figure 5).

Conversely, in recurrent tumors, CTNNA3, MBP, and COL3A1 demonstrated negative correlations with patient survival, indicating that higher expression levels are associated with shorter survival times in the recurrent setting (Figure 5). This relationship was most pronounced for CTNNA3 and MBP, which showed moderate negative correlations (Spearman $\rho < -0.3$) with marginal significance ($p < 0.1$), suggesting these genes may play context-dependent roles in GBM progression.

DOI: 10.54254/2753-8818/2025.AU27080

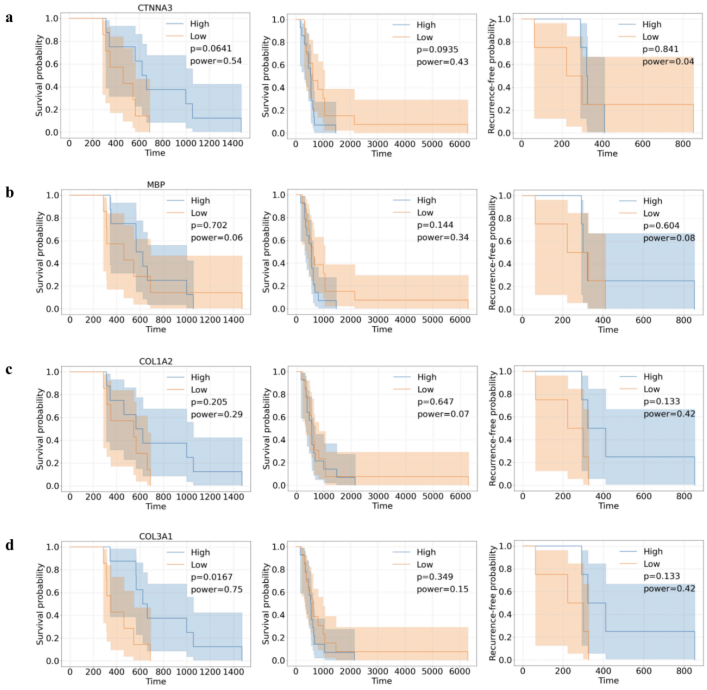


Figure 6. Kaplan-Meier survival curves for (a) CTNNA3, (b) MBP, (c) COL1A2, and (d) COL3A1. Left column: survival probabilities by gene expression in primary tumors (n = 15). Middle column: survival probabilities by gene expression in recurrent tumors (n = 27). Right column: recurrence-free probability by gene expression in primary tumors (n = 8). For each gene, patients were stratified into high (blue) and low (orange) expression groups in comparison to median gene expression. P-values indicate statistical significance between high and low expression groups determined by log-rank test

In primary tumors, elevated expression of CTNNA3, COL1A2, and COL3A1 was associated with improved overall survival probabilities, although these associations did not reach statistical significance (Figure 6). In contrast, and consistent with our correlation analyses, higher expression of CTNNA3 and MBP in recurrent tumors was predictive of higher recurrence-free probabilities ($p < 0.15$) (Figure 6). Finally, elevated primary expression of all four genes (CTNNA3, MBP, COL1A2, and COL3A1) corresponded to higher recurrence-free probability within 300 days. The limited statistical power observed for primary CTNNA3 expression versus recurrence time (power = 0.04) and primary MBP expression versus survival time (power = 0.06) can be partly attributed to the small sample sizes of 8 and 15 patients, respectively.

DOI: 10.54254/2753-8818/2025.AU27080

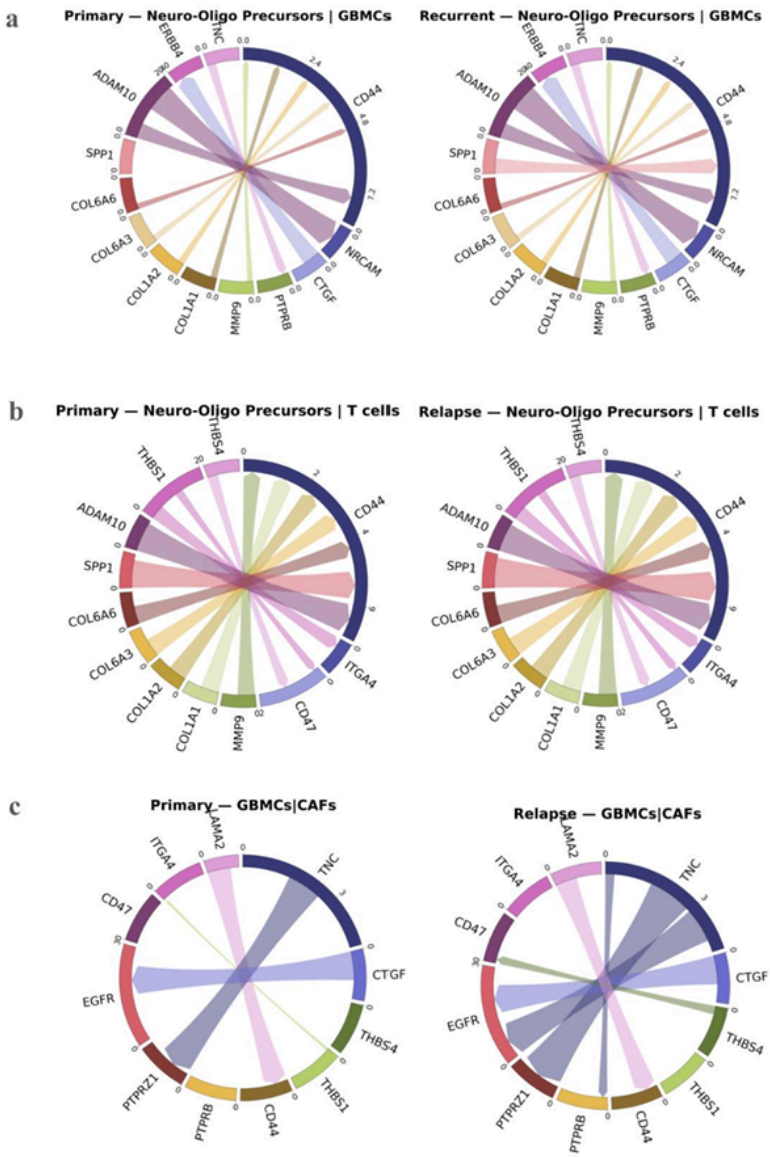


Figure 7. Circos plots demonstrating ligand-receptor interactions between cell types in primary (left) versus recurrent (right) tumors for: (a) neuro-oligo precursor cells (OPCs) and GBM cells, (b) OPCs and T cells, and (c) GBM cells and cancer-associated fibroblasts (CAFs). Arrow width represents interaction strength (coexpression coefficient). Only statistically significant interactions are displayed

Cell-cell communication analysis revealed changes in extracellular matrix signaling networks during GBM progression. Between neuro-oligo precursor cells and GBM cells, a novel significant interaction emerged between SSP1 and CD44 in recurrent tumors (coexpression = 0.572, $p < 0.05$), while most existing interactions were strengthened in recurrent versus primary tumors, with the notable exception of decreased ADAM10-CD44 coexpression (Figure 7a). SSP1 is an ECM glycoprotein whose coupled interaction with CD44 has been found to drive glioma progression by promoting signaling between cancer cells and macrophages [15]. This novel interaction could promote ECM remodeling and contribute to aggressive phenotypes in relapsed GBM. Similarly, OPC-T cell communications were generally enhanced in recurrent tumors, except for reduced

DOI: 10.54254/2753-8818/2025.AU27080

THBS1-ITGA4 and ADAM10-CD44 interactions (Figure 7b). Most dramatically, GBM cell interactions with cancer-associated fibroblasts showed three novel significant interactions in recurrent tumors: EGFR-TNC (coexpression = 1.112), THBS4-CD47 (coexpression = 0.272), and PTPRB-TNC (coexpression = 0.290), indicating extensive remodeling of the tumor microenvironment during recurrence (Figure 7c).

3.2. Experimental results validate computational analysis

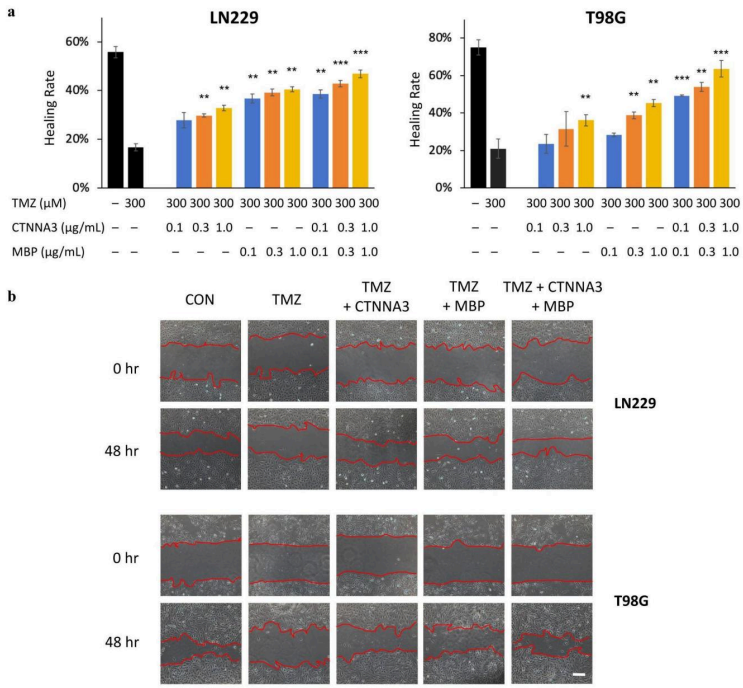


Figure 8. (a) Healing rate of LN229 (left) and T98G (right) cells after 48 hours of treatment with 300 μg/mL TMZ and recombinant proteins (0.1 μg/mL: blue, 0.3 μg/mL: orange, 1.0 μg/mL: yellow). Black bars: negative control and TMZ-only control. Bars represent mean ± SD (n = 3). *p < 0.05, **p < 0.01, ***p < 0.001 vs TMZ control. (b) Wound healing images at 0 and 48 hours. Cells treated with 300 μg/mL TMZ and 1 μg/mL recombinant protein. Red lines mark wound boundaries. Scale bar = 100 μm

Wound healing assay confirmed that CTNNA3 and MBP enhance GBM cell migration in a dose-dependent manner. Both LN229 and T98G cell lines treated with recombinant CTNNA3 and MBP proteins showed significantly increased wound healing rates compared to TMZ-only controls (Figure 8). The most pronounced effect was observed with combined treatment at 1.0 μg/mL, where healing rates increased approximately threefold in LN229 cells (46.93% vs 16.67% for TMZ control, $p < 0.001$) as well as in T98G cells (63.57% vs 20.98% for TMZ control, $p < 0.001$) (Figure 8a). A dose-dependent effect was observed, with progressive increases in migration at higher protein concentrations and statistical significance achieved at concentrations ≥ 0.3 μg/mL for most treatment groups.

DOI: 10.54254/2753-8818/2025.AU27080

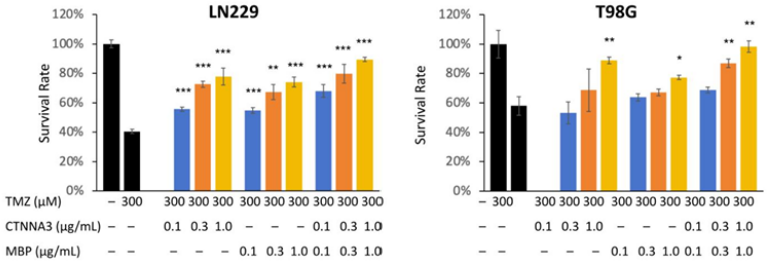


Figure 9. Survival rates of LN229 (left) and T98G (right) cell lines under identical treatment conditions as the wound healing assay. Cells were treated with 300 μg/mL TMZ and CTNNA3, MBP, or both recombinant proteins (0.1 μg/mL: blue, 0.3 μg/mL: orange, 1.0 μg/mL: yellow). Black bars: negative control and TMZ-only control. Bars represent mean ± SD (n=3). *p < 0.05, **p < 0.01, ***p < 0.001 vs TMZ control

Cell viability assays demonstrated that CTNNA3 and MBP treatment significantly enhanced GBM cell survival under TMZ treatment conditions. Both cell lines exhibited dose-dependent increases in survival rates, with the highest concentrations (1.0 μg/mL) of combined CTNNA3 and MBP treatment resulting in more than twice the survival rate of TMZ controls in LN229 cells and 1.5-fold higher survival in T98G cells (Figure 9). These findings indicate that beyond restoring healing rate, CTNNA3 and MBP also confer resistance to chemotherapy-induced cell death, potentially contributing to treatment failure in recurrent GBM.

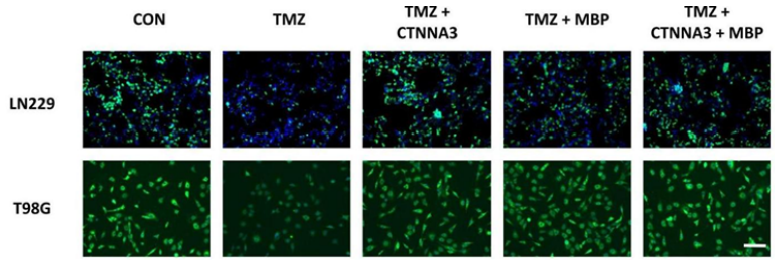


Figure 10. Immunofluorescence analysis of collagen IV expression in (a) LN229 and (b) T98G cell lines treated with TMZ and 1.0 μg/mL of CTNNA3, MBP, or both recombinant proteins. Green fluorescence: collagen IV. Blue: DAPI-stained nuclei. Images captured at 200× magnification. Scale bar = 100 μm

Immunofluorescence analysis revealed that CTNNA3 and MBP treatment significantly increased ECM protein production. Both LN229 and T98G cells showed enhanced collagen IV expression following recombinant protein treatment, with the most intense fluorescence observed in cells treated with both CTNNA3 and MBP simultaneously (Figure 10).

4. Discussion

Recurrent GBM represents a significant challenge in cancer treatment as 90% of patients within 2 years of initial surgery [1, 4]. Our analysis revealed that neuro-oligo precursor cells represent a key population in relapsed GBM, with CTNNA3 and MBP serving as critical mediators of ECM restructuring and therapy resistance. Rather than directly driving GBM relapse, these factors contribute to treatment resistance in established recurrent.

Our dimensional reduction analysis revealed that the neuro-oligo precursor cluster is predominantly composed of relapsed GBM cells, suggesting their critical role in disease

DOI: 10.54254/2753-8818/2025.AU27080

progression. Wang et al. have reported how minimal development of DNA mutations specific to GBM recurrence may suggest that instead of genetic evolution, phenotype switch may underly failure of GBM therapies [8, 16]. Our findings complement this understanding by identifying a specific cellular population that potentially facilitates this phenotypic alteration. Unlike Wang et al.'s focus on proneural-to-mesenchymal transitions in bulk tumor populations, our study specifically characterizes the neuro-oligo precursor population, which are similar to cancer stem cells in their ability to self-renewal and differentiate, rendering them crucial for tumor progression [8, 17]. The "niche" formed by neuro-oligo precursors provides a protective microenvironment that promotes survival of recurrent tumors. While Wang et al. identified increased T-cell abundance and mesenchymal shift at recurrence, our analysis specifically links the neuro-oligo precursor population to enhanced invasive capacity of recurrent GBM through their self-renewal and migrational abilities [8, 18].

Differential expression analysis identified CTNNA3 and MBP among the top upregulated genes in relapsed GBM, with both proteins associated with enhanced cell adhesion and migration capabilities [10, 11]. However, our survival analysis revealed an unexpected pattern where higher CTNNA3 and MBP expression correlated with longer survival in primary tumors but consistently marked more aggressive, treatment-resistant states in relapsed patients. This counterintuitive relationship demonstrates that while CTNNA3 & MBP do not directly drive tumor recurrence, they serve as critical determinants of treatment efficacy once relapse has occurred. In primary contexts, CTNNA3 and MBP expression may reflect retention of normal structural functions, while their upregulation in relapse specifically marks cellular populations with enhanced therapeutic resistance that renders recurrent tumors more resistant to standard treatments.

Machine learning analysis further identified FBXO2, CLEC2A, and CAPN13 as top predictors of relapse, with FBXO2's role in cancer cell migration and metastasis in colorectal cancer supporting its relevance to GBM invasiveness [12]. CLEC2A evokes immune responses through regulation of dendritic cell migration and adhesion [13]. The calpain family of proteases has been implicated in cellular motility [14]. Thus, computational analysis collectively reveals the relevance of the tumor microenvironment to relapsed GBM cells, highlighting the role of CTNNA3 and MBP genes. This computational framework differs from previous approaches by identifying specific molecular signatures that distinguish relapsed from primary disease states.

Our wet laboratory results validate computational findings using LN229 and T98G GBM cell lines. LN229 and T98G are established GBM cell lines that demonstrate reliable growth, making them suitable experimental models for the robust recurrent GBM cells. Treating these cell lines with TMZ reduced migration, proliferation, and ECM protein expression, consistent with chemotherapy-induced cellular stress. However, supplementation with CTNNA3 and MBP recombinant proteins restored these abilities, aligning with our observation that high CTNNA3 and MBP expression in relapsed tumors negatively correlated with survival in the correlation and survival analysis. Wound healing and CCK-8 assays confirmed that CTNNA3 and MBP enhance GBM cell migration and survival abilities. Stronger cell-cell adhesion likely creates physical barriers that impede chemotherapy access and render cells more resilient. While no prior studies have directly linked CTNNA3 or MBP to chemoresistance, previous research has shown that other adhesion molecules, such as HSF2, protect cells under stress conditions by maintaining protein stability [19]. This suggests that enhanced adhesion may also prevent TMZ-induced apoptosis through activation of signaling cascades associated with cell adhesion and stress response.

Our immunofluorescence analysis further supports the role of CTNNA3 and MBP in extracellular matrix (ECM) remodeling and therapy resistance. TMZ reduced the fluorescence of collagen IV, but

DOI: 10.54254/2753-8818/2025.AU27080

the restored fluorescence of collagen IV in cells treated with recombinant proteins suggests that CTNNA3 and MBP promote ECM stiffening, which may help create a protective niche against TMZ-induced stress. Previous studies have shown that in breast cancer, a denser ECM can enhance collective migration and invasion by providing structural support for tumor cells, allowing them to navigate the tumor microenvironment more efficiently [20]. Similarly, CTNNA3 and MBP may contribute to modifying the tumor microenvironment to better suit the proliferation of relapsed GBM cells.

We acknowledge limitations on our survival analysis by sample size, which reduced statistical power to detect significant associations between gene expression and clinical outcomes. We also acknowledge limitations of our experimental validation, as it relied primarily on established GBM cell lines (LN229 and T98G) cultured in petri dishes, which does not capture the complexity of real-world three-dimensional tumors. Increasing sample size and in vivo experiments are necessary for enhanced understanding of GBM relapse. Future therapeutic strategies should investigate the effects of specifically silencing CTNNA3 and MBP expression, potentially incorporating these targets into combinatorial treatment approaches designed to disrupt the protective tumor microenvironment in relapsed GBM. Additionally, researchers could target the self-renewal and differentiation mechanisms of neuro-oligo precursors, given their substantial representation within relapsed tumor populations. Our computational analysis has also identified other promising candidates, including PLP1, FBXO2, and MALAT1, which may also be significant to recurrent GBM.

Through scRNA-seq analysis, we identified a significant population of neuro-oligo precursors among relapsed GBM cells, demonstrating their role in establishing "protective tumor niches" to confer treatment resistance. Through experimental validation, we confirmed that CTNNA3 and MBP recombinant proteins restore migration, survival, and ECM protein expression capabilities in TMZ-treated GBM cells. The integration of computational and experimental approaches in our study establishes a robust framework for identifying and functionally validating therapeutic targets in GBM relapse. Our study provides a foundation for future therapeutic strategies targeting cellular and molecular mechanisms underlying recurrent GBM, potentially offering new avenues to overcome treatment resistance and improve patient outcomes.

Acknowledgement

I want to express my gratitude toward Dr. Zhang, whose advice has been of great value in my research process. I also would like to sincerely thank Dr. Wu and all of my teachers for inspiring me to remain curious and for nurturing my passion in science and biology. Thank you to my parents and my friends, for having my back at every turn of this long journey. Finally, a special thanks to Wang et al. for publishing the single cell dataset of human glioma which enabled this research.

References

[1] Miele, E., Anghileri, E., Calatozzolo, C., Lazzarini, E., Patrizi, S., Ciolfi, A., … & Pollo, B. (2024). Clinicopathological and molecular landscape of 5-year IDH-wild-type glioblastoma survivors: A multicentric retrospective study. Cancer letters, 588, 216711. https: //doi.org/10.1016/j.canlet.2024.216711

[2] Grech, N., Dalli, T., Mizzi, S., Meilak, L., Calleja, N., & Zrinzo, A. (2020). Rising Incidence of Glioblastoma Multiforme in a Well-Defined Population. Cureus, 12(5), e8195. https: //doi.org/10.7759/cureus.8195

[3] Rodgers, L. T., Villano, J. L., Hartz, A. M. S., & Bauer, B. (2024). Glioblastoma Standard of Care: Effects on Tumor Evolution and Reverse Translation in Preclinical Models. Cancers, 16(15), 2638. https: //doi.org/10.3390/cancers16152638

[4] Minniti, G., Niyazi, M., Alongi, F., Navarria, P., & Belka, C. (2021). Current status and recent advances in reirradiation of glioblastoma. Radiation Oncology, 16(36). https: //doi.org/10.1186/s13014-021-01767-9

DOI: 10.54254/2753-8818/2025.AU27080

[5] Jovic, D., Liang, X., Zeng, H., Lin, L., Xu, F., & Luo, Y. (2022). Single-cell RNA sequencing technologies and applications: A brief overview. Clinical and Translational Medicine, 12(3): e694. https: //doi.org/10.1002/ctm2.694
[6] Wu, X., Yang, B., Udo-Inyang, I., Ji, S., Ozog, D., Zhou, L., & Mi, Q. (2018). Research Techniques Made Simple: Single-Cell RNA Sequencing and its Applications in Dermatology. Journal of Investigative Dermatology, 138(5), 1004-1009. https: //doi.org/10.1016/j.jid.2018.01.026
[7] Wen, L., Li, Y., Li, S., Gou, Y., Duan, Y., Liu, B., … & Zhang, X. (2023). Advances in single-cell RNA sequencing and its applications in cancer research. Journal of Hematology & Oncology, 16(98). https: //doi.org/10.1186/s13045-023-01494-6
[8] Wang, L., Jung, J., Babikir, H., Shamardani, K., Jain, S., Feng, X., … & Diaz, A. A. (2022). A single-cell atlas of glioblastoma evolution under therapy reveals cell-intrinsic and cell-extrinsic therapeutic targets. Nature Cancer 3, 1534–1552. https: //doi.org/10.1038/s43018-022-00475-x
[9] Janssens, B., Mohapatra, B., Vatta, M., Goossens, S., Vanpoucke, G., Kools, P., … & Towbin, J. A. (2003). Assessment of the CTNNA3 gene encoding human alpha T-catenin regarding its involvement in dilated cardiomyopathy. Human Genetics, 112(3), 227-236. https: //doi.org/10.1007/s00439-002-0857-5
[10] Janssens, B., Goossens, S., Staes, K., Gilbert, B., van Hengel, J., Colpaert, C., … & van Roy, F. (2001). αT-catenin: a novel tissue-specific β-catenin-binding protein mediating strong cell–cell adhesion. Journal of Cell Science, 114(17), 3177-3188. https: //doi.org/10.1242/jcs.114.17.3177
[11] Boggs, J.M. (2006). Myelin basic protein: a multifunctional protein. Cell Mol Life Sci, 63(17), 1945-1961. https: //doi.org/10.1007/s00018-006-6094-7
[12] Wei, X., Bu, J., Mo, X., Lv, B., Wang, X., & Hou, B. (2018). The prognostic significance of FBXO2 expression in colorectal cancer. International journal of clinical and experimental pathology, 11(10), 5054–5062.
[13] de Winde, C. M., Matthews, A. L., van Deventer, S., van der Schaaf, A., Tomlinson, N. D., Jansen, E., … & van Spriel, A. B. (2018). C-type lectin-like receptor 2 (CLEC-2)-dependent dendritic cell migration is controlled by tetraspanin CD37. Journal of cell science, 131(19), jcs214551. https: //doi.org/10.1242/jcs.214551
[14] Franco, S. J., & Huttenlocher, A. (2005). Regulating cell migration: calpains make the cut. Journal of cell science, 118(Pt 17), 3829–3838. https: //doi.org/10.1242/jcs.02562
[15] He, C., Sheng, L., Pan, D., Jiang, S., Ding, L., Ma, X., … & Jia, D. (2021). Single-cell transcriptomic analysis revealed a critical role of SPP1/CD44-Mediated crosstalk between macrophages and cancer cells in glioma. Frontiers in cell and developmental biology, 9, 779319. https: //doi.org/10.3389/fcell.2021.779319
[16] Barthel, F. P., Johnson, K. C., Varn, F. S., Moskalik, A. D., Tanner, G., Kocakavuk, E., … & GLASS Consortium. (2019). Longitudinal molecular trajectories of diffuse glioma in adults. Nature, 576(7785), 112–120. https: //doi.org/10.1038/s41586-019-1775-1
[17] Akay, L. A., Effenberger, A. H., & Tsai, L. H. (2021). Cell of all trades: oligodendrocyte precursor cells in synaptic, vascular, and immune function. Genes & development, 35(3-4), 180–198. https: //doi.org/10.1101/gad.344218.120
[18] Decker, L., Avellana-Adalid, V., Nait-Oumesmar, B., Durbec, P., & Baron-Van Evercooren, A. (2000). Oligodendrocyte precursor migration and differentiation: Combined effects of PSA residues, growth factors, and substrates. Molecular and Cellular Neuroscience, 16(4), 422–439. https: //doi.org/10.1006/mcne.2000.0885
[19] Joutsen, J., Da Silva, A. J., Luoto, J. C., Budzynski, M. A., Nylund, A. S., de Thonel, A., Concordet, J. P., Mezger, V., Sabéran-Djoneidi, D., Henriksson, E., & Sistonen, L. (2020). Heat shock factor 2 protects against proteotoxicity by maintaining cell-cell adhesion. Cell reports, 30(2), 583–597.e6. https: //doi.org/10.1016/j.celrep.2019.12.037
[20] Koorman, T., Jansen, K. A., Khalil, A., Haughton, P. D., Visser, D., Rätze, M. A. K., … & Derksen, P. W. B. (2022). Spatial collagen stiffening promotes collective breast cancer cell invasion by reinforcing extracellular matrix alignment. Oncogene, 41(17), 2458–2469. https: //doi.org/10.1038/s41388-022-02258-1